Applied Surface Science 638 (2023) 157967

Contents lists available at ScienceDirect

Applied Surface Science

journal homepage: www.elsevier.com/locate/apsusc

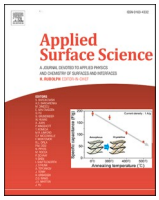

Full Length Article

Reducing specific contact resistivity for n-type germanium using laser activation process and nano-island formation

Seunghun Baik [a], Heejae Jeong [a], Geuntae Park [a], Hongki Kang [a], Jae Eun Jang [a], Hyuk-Jun Kwon [a,b,*]

[a] Department of Electrical Engineering and Computer Science, DGIST, Daegu 42988, South Korea
[b] Convergence Research Advanced Centre for Olfaction, DGIST, Daegu 42988, South Korea

ARTICLE INFO

Keywords:
Ge
Phosphorus
CMOS
Laser activation
Triple contact
Specific contact resistivity

ABSTRACT

This study presents a laser activation process (LAP) for germanium (Ge) to improve the electrical performance of n-type Ge devices. The LAP highly activated the dopant and created a shallow junction in Ge. We also investigated a triple contact of titanium (Ti)/nickel (Ni) nano-island/Ge to reduce contact resistivity and enhance the tunneling current. The results showed that the LAP with a fluence of 140 mJ/cm^2 effectively activated the dopant, resulting in a high forward current density and a low ideality factor of the n$^+$-p junction diode. The triple contact of Ti/Ni nano-island/Ge showed the lowest specific contact resistivity, indicating an increase in the tunneling current. The Ni nano-island contact showed the best overall electrical performance, attributed to the boosted electric field and the lower density of states at the interface. The results show that combining multiple approaches, including the optimized laser activation process and triple contact formation, can significantly reduce the contact resistance on n-type Ge, providing a promising approach for improving performance.

1. Introduction

Rapid advances in Information Technology (IT) have driven semiconductor engineering to continuously reduce transistor size to meet the constant demand for higher density and performance [1]. The creation of smaller devices has followed Moore's Law, which has seen the doubling of transistor density every two years. Scaling transistor dimensions has been sufficient for technology nodes longer than 90 nm. However, as nodes shrank below this threshold, new ideas, such as high-k gate dielectric, fin field-effect transistor (FinFET) architecture, silicon-germanium (SiGe) Channel, and front-end-of-line (FEOL) engineering, were developed to achieve technology nodes as small as 10 nm and extend Moore's Law [2–4]. However, scaling alone is no longer sufficient to achieve nodes below 7 nm, due to velocity saturation, which limits the mobility of the drain current. To address this, the shift to high-mobility channels such as germanium (Ge) is expected to occur by 2028, according to IRDS: 2021 [5].

Ge exhibits several promising properties that make it a potential replacement for silicon (Si) in future complementary metal-oxide semiconductor (CMOS) technology, including a high hole mobility of 1,900 cm^2/Vs and moderate electron mobility of 3,900 cm^2/Vs, a low processing temperature, and high carrier density when compared to III-V materials. However, the commercialization of Ge is impeded by a significant obstacle: the proportion of contact resistance in the total source/drain series resistance is higher at a metal and Ge semiconductor interface [6]. Also, n-type Ge suffers serious fermi-level pinning which results in a higher Schottky barrier, limiting the tunneling current [7–9]. Accordingly, achieving highly doped Ge for efficient device performance remains a challenge in CMOS applications, with one of the major obstacles being the difficulty in obtaining low contact resistance for Ge.

Achieving low specific contact resistivity (ρ_c) for Ge is a particularly significant challenge when the concentration of n-type dopants (N_D) is boosted because this affects the contact resistance. Although phosphorus (P) is a promising n-type dopant with a low activation energy and an expectedly high solubility limit, the concentration of activated P in Ge is limited to approximately $\sim 5 \times 10^{19}$ cm^{-3}, lower than the theoretical maximum solubility of P in Ge, which is 6×10^{20} cm^{-3}. The fabrication of high-quality Ge devices requires precise control of doping profiles, which is difficult because the dopants rapidly diffuse in Ge [10,11]. To overcome the limitation, several approaches were made on the issue. To suppress the diffusion of P, co-doping effects were studied. Introducing other dopant species, such as antimony (Sb) and fluorine (F) retarded P

* Corresponding author at: Department of Electrical Engineering and Computer Science, DGIST, Daegu 42988, South Korea.
E-mail address: hj.kwon@dgist.ac.kr (H.-J. Kwon).

https://doi.org/10.1016/j.apsusc.2023.157967
Received 13 May 2023; Received in revised form 20 June 2023; Accepted 3 July 2023
Available online 5 July 2023

diffusion due to reduced interstitial vacancies and local strain compensation due to large atomic radius [12–14]. To make an atomically clean contact layer, in-situ activation while epitaxial growth by chemical vapor deposition with P was studied. The crystalline layer was achieved by the process minimized the defects boosting efficiency of doped P [15]. One promising technique for achieving a suitable concentration of highly activated dopant in Ge is the laser activation process (LAP). LAP involves rapid heating and cooling, which enables a high degree of dopant activation as well as control of the dopant diffusion profiles [16]. Introducing interlayer and germanidation at the contact interface were tried for lower contact resistance even with low P concentration. The interlayer of dipoles lowered Schottky barrier height, minimizing metal-induced gap states [17]. Germanidation significantly decreased the ρ_c with low-resistive phase, making it easier for carriers to cross the interface [18].

In this study, we present a detailed investigation of LAP with Ge and P as dopants using a pulsed laser. We analyze the dopant concentration, sheet resistance (R_s), and ρ_c of metal-Ge contacts to understand the activation behavior of P in Ge.

Previously it was determined that the low P concentration at the surface of Ge after activation was due to a vacancy-mediated diffusion process via P cluster formation, which led to fast diffusion during the annealing process used for activation [19–21]. This process represents a bottleneck to further reduction in contact resistance, mainly because of the large Schottky barrier. To avoid this issue, the dopant delivery and pulsed laser activation and recrystallization steps must be optimized. During pulsed laser activation, solid-phase epitaxy (SPE) occurs, forming a metastable alloy of P and Ge, resulting in high dopant concentrations that can even exceed the solubility limit [22–24].

In this study, we aimed to enhance the metallurgical reactions observed in Ge to improve device performance caused by poor thermal stability, rough surfaces, and dopant consumption issues [25–27]. Specifically, we employed a contact modification technique using metal nano-particle formation, that involves the insertion of metal nano-islands at the contact area to enhance the electric field at the metal–semiconductor (MS) interface, and reduce the effective barrier height [28–30]. The small metal nanoparticles act as the small patches at the MS interface, allowing a saddle point potential effect. The target materials were selected based on their compatibility with CMOS fabrication, the need for a high difference in work function between the two metals, and the ability to deposit or form the nano-islands using conventional deposition processes.

To this end, we chose nickel (Ni) as the nano-island material and titanium (Ti) as the contact material because their work functions are well-matched with Ge according to the Schottky-Mott rule, with a work-function difference of approximately 1 eV. The workfunction difference between Ni and Ti leads to a charge transfer and enhances an electrical field. Additionally, Ni and Ti are CMOS-compatible metals, simplifying fabrication. We investigated the use of the Ti/Ni nano-island/activated Ge triple contact as an alternative to Ni germanidation.

This study aimed to achieve lower Ge contact resistance by combining the effects of field enhancement, provided by the nano-island formation, with the high dopant concentration, for a single contact interface with low ρ_c. The fabrication of the n-type Ge was evaluated with a focus on determining the optimal condition of the LAP and the Ti/Ni nano-island/activated Ge triple contact, which was shown to improve device performance by reducing contact resistance. By combining these approaches, the potential of Ge in CMOS technology can be fully realized.

2. Experimental methods

Fig. 1 presents a schematic of the process sequence for activating dopants and forming nano-island contacts to achieve a low resistive contact. The reduction in contact resistance is attributed to an increase in tunneling current. Thinner and lower Schottky barrier heights are crucial to increasing tunneling current and decreasing tunneling resistance. The sample used for the experiment was a 4-inch monocrystalline wafer of lightly Gallium (Ga) doped p-type Ge (1 0 0) with a resistivity of 1 Ω•cm. P ions were implanted at an energy of 15 keV with a dose of 1×10^{16} cm^{-2} and a tilting angle of 7° at room temperature. After ion implantation, the Ge wafer was cleaned with acetone and isopropanol alcohol to remove organic residue and particles and blown with pure nitrogen gas. A 100 nm thick SiO_2 film was then deposited on the Ge wafer using plasma-enhanced chemical vapor deposition (PE-CVD). The wafer was cut into 1 cm × 1 cm sized square coupons for convenience.

For the activation process, a 30-nanosecond pulsed laser with a wavelength of 355 nm and a repetition frequency of 70 kHz (AVIA 355-X, Coherent) was performed at a scanning speed of 1 mm/s on the sample with nano-positioning stages. The energy density was converted from the measured power and optimized to minimize surface damage while activating the dopants. The Gaussian laser beam was shaped into a 150 μm × 10 μm Top-Hat line beam for uniform intensity using a diffractive optical element and a focusing objective lens with a magnification of 10. Note that the LAP was performed under air ambient.

The depth profile of the chemical dopant concentrations was measured using time-of-flight secondary ion mass spectrometry (ToF-SIMS) with an iONTOF TOF.SIMS 5 instrument. A 1 keV caesium$^+$ (Cs^+) beam was sputtered for depth profiling, and a primary beam with bismuth (Bi) was applied for spectrometry. The Cs^+ beam was rastered over a 300 μm × 300 μm area on the surface, while the Bi beam was aligned at the center. For depth calibration, the sputtered depth was measured by atomic force microscopy (AFM). The active dopant concentration was measured by scanning spreading resistance microscopy (SSRM). For

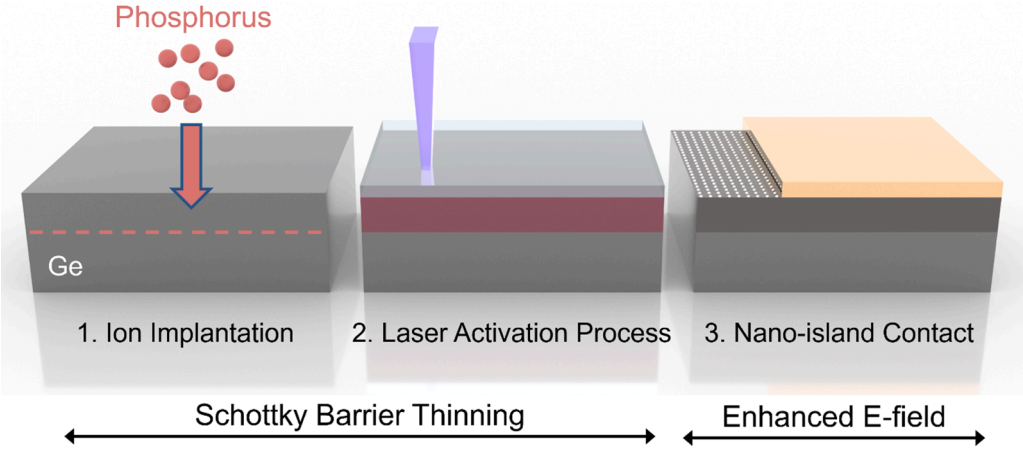

Fig. 1. A schematic of the process steps for laser activation and nano-island contact.

SSRM, the coupons were polished in a cross-sectional view to make the surface very smooth. The crystalline quality of the Ge wafer before and after laser activation was characterized using high-resolution transmission electron microscopy (HR-TEM) with an FEI Themiz Z. Cross-sectional samples were prepared using a focused ion beam (FIB) with a Helios NanoLab G3 UC instrument. The sheet resistance was measured using the 4-point probe method. To evaluate the laser activation by electrical conductivity, 100 μm × 100 μm sized metal contacts were deposited on top of the activated Ge with a 100 μm distance gap. For the metal contact, 150 nm thick Ti was deposited and patterned by a lift-off process in acetone.

Following the LAP, nano-island embedded contacts were deposited using a DC sputtering system. The material characterization of the triple contact nanoscale formation was conducted using HR-TEM in energy dispersive spectroscopy (EDS) mode. The multi-ring circular transmission line method (MR-CTLM) was employed to determine the ρ_c.

For the n^+-p diode structure, top-contact metal structures were used to measure the current, while the back contact was located on the bottom of the Ge wafer. A 300 nm thick aluminum (Al) film was deposited using a direct current (DC) sputtering system to form the back contact. The electrical results were measured using a semiconductor parameter analyzer, Keithley 4200-SCS.

3. Results and discussion

3.1. Highly activated n-Ge with pulsed laser activation process

Fig. 2 (a) describes the use of a line beam with flat top-hat intensity to minimize surface damage and achieve a higher dopant concentration during the laser activation process. The laser beam is first shaped into a line beam using a diffractive optical element (DOE) after being controlled by a polarizing component with a wave plate. The intensity profile of the line beam had a length of 150 μm and a width of 10 μm where the intensity was higher than 50% of the peak value. The intensity of the laser beam was measured by Si-based image sensors.

Compared to a Gaussian laser beam, which ablates a substrate due to the high energy distribution at the center of the beam, the line beam damages the sample less because of its constant power uniformity. The line beam also allows a wider annealing area and uniformly activates the dopants, which is essential for low resistance in the contact area. Fig. 2 (b) provides an HR-TEM image after the laser activation process was performed without removing the capping layer, showing a recrystallized layer of about 33 nm thickness without any damaged areas. The 100 nm thick SiO_2 capping layer prevents out-diffusion during the activation process and boosts the annealing effect with a blanket-like effect. However, the capping layer is fragile and an annealing process can break it down. The line beam avoids damage to the capping layer, even after the activation and recrystallization of the P-implanted layer.

ToF-SIMS is a technique used to analyze the chemical composition of materials. In this case, it was used to analyze the degree of LAP in the samples. The P concentration profiles of the implanted samples activated under different conditions are plotted in Fig. 3 (a). The as-implanted sample showed a peak dopant concentration of 8.4 × 10^{20} atoms/cm^3 at 12 nm below the surface. The dopant profile showed a steep slope at 25 nm deep due to the dopants collision with Ge atoms, which caused the dopants to lose the power to drive further in.

LAP results with an energy density of 140 mJ/cm^2 showed diffuseless results with dopant distributions identical to the as-implanted sample. At an energy density of 170 mJ/cm^2, the slope of the dopant distribution slightly decreased compared to the results for the lower energy LAP case, due to diffusion of the dopants. Diffusion behavior was found at higher energy densities of 210 mJ/cm^2 and 250 mJ/cm^2. As the dopants diffused into the substrate, the peak dopant concentration decreased proportionally to the diffusion depth. For comparison, two rapid thermal proces (RTP) conditions are also presented in Fig. 3 (a). RTPs of 500 °C and 600 °C were performed under N_2 ambient for 1 min. After the RTP of 500 °C, the dopants were diffused through the substrate, lowering the peak dopant concentration due to the fast diffusion characteristic of P in Ge. After the RTP of 600 °C, most of the dopants had diffused through the Ge substrate.

In order to gain insight into the diffusion behavior of dopants in Ge, it is necessary to examine the diffusion profile following the dopant-delivering step, and the annealing step. In this study, two process steps were employed: ion implantation with low-energy delivered dopants, followed by LAP to activate the dopants in the Ge lattice. A capping layer to prevent the out-diffusion of dopants was assumed, and the total number of injected dopants was considered to be constant. Under these conditions, the diffusion profile after annealing can be described by Eq. (1) [31],

$$C(x) = \left(\frac{2C_0}{\pi}\right)\bullet\left(\frac{Depth_I}{D_a t_a}\right)^{\frac{1}{2}} \bullet e^{\frac{-x^2}{4D_a t_a}} \quad (1)$$

where C(x) represents the diffusion profile with a depth coordinate of x, C_0 is the concentration of dopants at the peak near the surface after ion implantation, $Depth_I$ is the injected depth of dopants by ion implantation process, D_a is the diffusion coefficient at the temperature of the annealing process, and t_a is the annealing time. The equation indicates that the diffusion depth of the dopants depends on the diffusion constant and the annealing time.

It was found that LAP, which only takes 30 ns for a laser shot, effectively prevents dopant diffusion compared to RTP, which takes at least a few seconds. This result indicates that LAP could be a promising technique for achieving highly localized and precise doping in Ge.

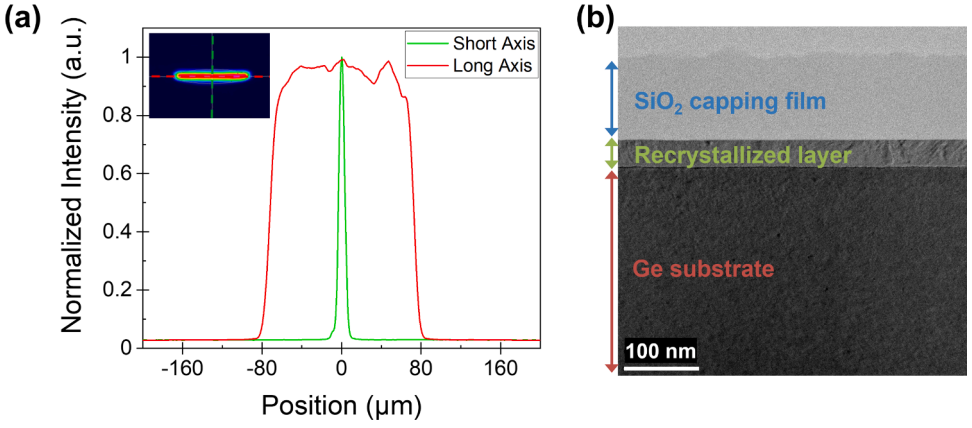

Fig. 2. (a) Measured intensity of a line beam with top-hat profile. (b) A HR-TEM image after LAP showing recrystallization of implanted layer and undamaged SiO_2 capping film.

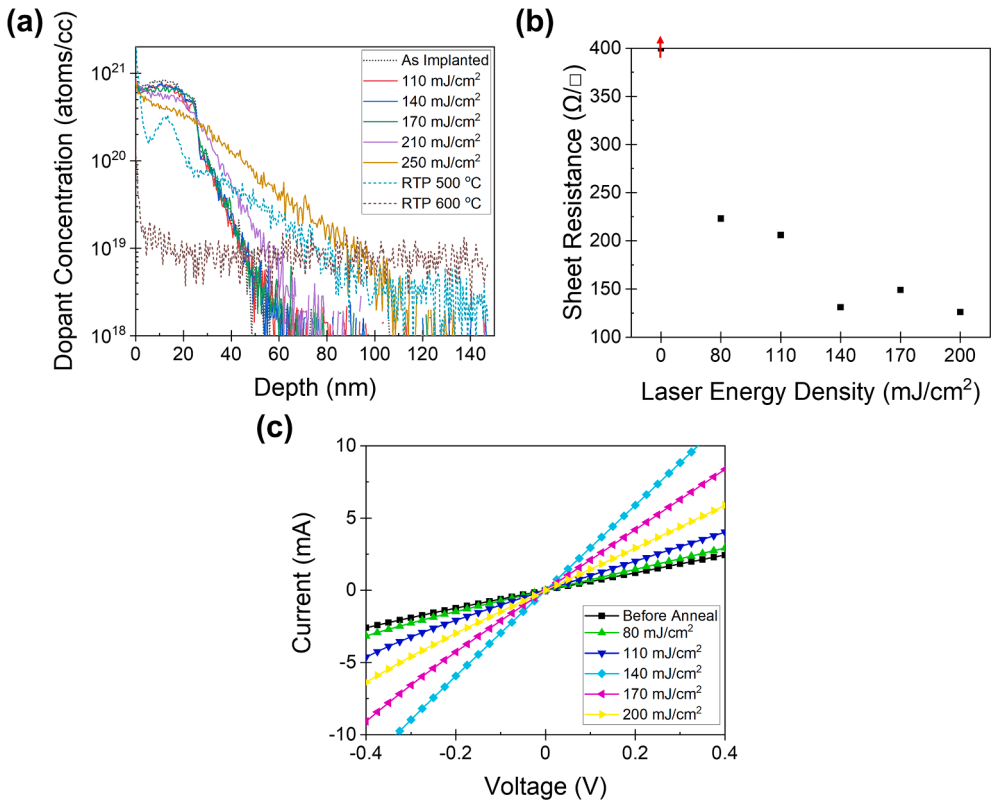

Fig. 3. (a) ToF-SIMS profile for P after LAP and RTP for various conditions. (b) Sheet resistance results after LAP. The result before LAP is indexed as 0 mJ/cm^2. (c) Two terminal I-V results after LAP. After 140 mJ/cm^2 of LAP, the result showed the most conductive result.

The use of LAP provides additional benefits beyond its fast heating time. The LAP also limits heating to the surface, leading to a limited thermal penetration depth. The thermal penetration depth is related to the thermal diffusivity and annealing time through the relation $d_{th} \approx 2\sqrt{D\tau}$, where d_{th} is the thermal penetration depth [32]. During annealing, the energy input is converted into local thermal energy and diffuses by thermal conduction driven by random vibrational motion. The area of the annealed region is critical to establishing the doping profile, since dopant diffusion is mainly mediated by thermally-activated processes. Consequently, the short-pulsed process creates a shallow isothermal layer, resulting in a steep temperature gradient. As a result, the dopants lose their drive-in energy, since the temperature decreases sharply with depth after the LAP process, minimizing dopant diffusion.

The effect of the LAP on electrical performance was evaluated by measuring the sheet resistance (R_s) of the samples, and the results are presented in Fig. 3(b). Before the LAP process, indicated as 0 mJ/cm^2, the R_s values were higher than 400 Ω/□ due to the inactivated dopants after the ion implantation process. As the energy density of the LAP increased, the Rs decreased, and the values reached 131 Ω/□ at 140 mJ/cm^2 and 126 Ω/□ at 200 mJ/cm^2. Ohmic contact behavior was also evaluated by performing I-V measurements on the Ti and n-type Ge contacts, and the results are shown in Fig. 3(c). Two metal contact pads were deposited on the activated area, and the current levels were measured at a distance of 100 μm between the pads. The results indicate that the LAP condition of 140 mJ/cm^2 resulted in the highest current levels compared to lower or higher energy density conditions.

It should be noted that although the R_s value was not the lowest at this energy density, it resulted in the most conductive I-V behavior. This can be explained by the fact that R_s is calculated by assuming a known and constant depth, which may not be the case for samples subjected to different energy densities of the LAP. Therefore, the dopant in the sample subjected to 200 mJ/cm^2 may have diffused more, resulting in a lower R_s value but lower electrical performance. Based on these results, it can be concluded that the LAP condition of 140 mJ/cm^2 is the most suitable for P activation in Ge, as it minimizes dopant diffusion while providing the highest electrical performance.

To investigate the recrystallization of the P-implanted amorphous layers, HR-TEM was used. Fig. 4 displays five representative conditions after the activation processes. Their resulting crystalline qualities were evaluated using a fast Fourier transform (FFT), which is displayed in the insets of the images. Before the activation process, an amorphous layer with a thickness of 33 nm was observed. The FFT image of the amorphous layer exhibited no focused spots, indicating the absence of periodic lattices at the atomic scale. Conversely, the substrate beneath the implantation layer displayed a highly crystalline layer with clear FFT results, indicating the periodic alignment of Ge atoms.

Recrystallization behavior was not observed in the implanted layer until the energy density reached 80 mJ/cm^2. Following laser annealing at 110 mJ/cm^2, the implanted layer displayed crystallinity in the HR-TEM and FFT images. The HR-TEM image exhibited a partially recrystallized layer that is polycrystalline with a small amorphous area at the bottom of the layer. The round-shaped amorphous spots were likely induced by thermal diffusion behavior between the implanted layer and Ge substrate [33].

At a higher LAP of 140 mJ/cm^2, a recrystallized layer without an amorphous layer between the implanted layer and the Ge substrate was observed, with clear, bright spots in the FFT analysis. However, at even higher energy densities, the crystallinity of the implanted layer started to deteriorate, and the crystallinity of the substrate was also damaged. Since the melting point of Ge is as low as 940 °C, the amorphous layer seems to have been a result of the laser's quenching effect. The LAP process increased the temperature in tens of nanoseconds and cooled at a comparable speed. As a result, the Ge layer was melted and cooled down before the Ge atoms could align into a crystal [34,35].

Fig. S1 shows unavoidable surface oxidation and increased roughness after an RTP of 600 °C for 1 min. The increased surface roughness is

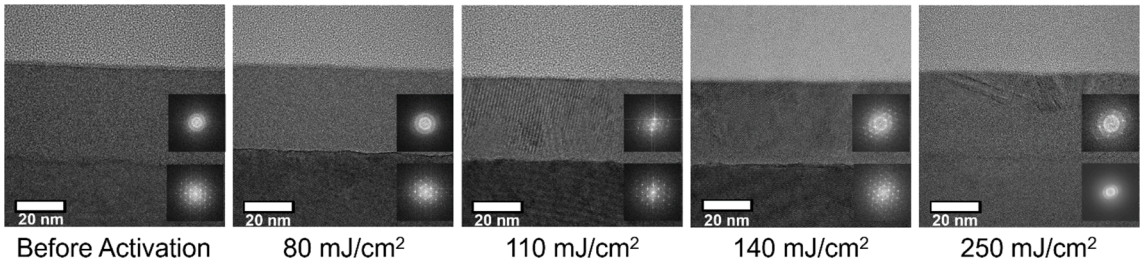

Fig. 4. HR-TEM images after various conditions of LAP. The inset figures are images from the FFT analysis, performed to confirm the quality of the recrystallized layer.

due to the fast diffusion behavior of Ge atoms, which not only recrystallized but were also re-distributed after RTP, which requires a longer heating duration. Fig. S2 shows the result of x-ray diffraction (XRD) measurement for Ge crytal peaks of the recystallized layers [36].

To investigate the relationship between chemical dopant concentration and active dopant concentration, we generated a comparative plot of ToF-SIMS and SSRM measurements for a LAP with an energy density of 140 mJ/cm^2 in Fig. 5 (a). As mentioned in Fig. 3 (a), the ToF-SIMS measurements revealed a peak dopant concentration of 7.79 $\times$ 10^{20} atoms/cm^3 with a corresponding junction depth of 48 nm meeting 5 $\times$ 10^{18} atoms/cm^3. In contrast, the SSRM measurements indicated an active dopant concentration of 2.98 $\times$ 10^{20} atoms/cm^3 and a shallower junction depth of 39 nm. This indicates that the LAP activated only 38% of the dopants. SSRM was performed using a conductive AFM tip with a few nanometers radius, by scanning the samples' cross-sections from the surface. The conductive tip measured the resistivity of the layer from the surface to the bottom, which allows the active carriers to be quantified in the depth profiling after the LAP. The SSRM conditions were carefully optimized, including measuring force, scanning speed, voltage bias, and sample thickness. Also, the calibration was taken before the measurement.

The high dopant concentration was likely due to the pulsed nature of the laser, which minimized thermal diffusion and helped preserve the crystal structure of the Ge wafer, as demonstrated in Figs. 3 and 4. Additionally, the high peak energy delivered by the laser activated the implanted dopants. Finally, the nanosecond-scale pulse duration of the laser partially melted and regrew the implanted layer by SPE. During LAP, atoms in the amorphous phase were locally rearranged at the interface between the crystalline and amorphous layers, which increased the dopant concentration through the SPE process [22–24,37].

Our study demonstrates that the SPE induced by the LAP allowed the active dopant concentrations to reach the maximum value under ideal solid solutions in equilibrium. Comparing the results of ToF-SIMS and SSRM measurements provides valuable insights into the distribution and activity of dopants in the material under investigation.

Fig. 5 (b) presents the results of the I-V measurements of Ti-activated Ge-Ti. The expected behavior of a metallic channel is a decrease in resistance as the temperature decreases, since there are fewer obstacles to the flow of electrons. The graph demonstrates that the highest conductivity was achieved at the lowest temperature of −180 °C. In Fig. S3 (a), the I-V measurement result after the LAP with a lower energy density shows decreased conductivity at a lower temperature. This indicates that the lower energy density of 110 mJ/cm^2 did not activate the dopants enough, causing the doped region to behave in a non-metallic way, with semiconducting characteristics.

In Fig. S3 (b), the higher energy density of 170 mJ/cm^2 of LAP resulted in metallic behavior. However, from −20 °C to −60 °C, the conductivity decreased, indicating that the crystal structure of the activated Ge layer was undergoing changes, which can decrease the number of available charge carriers [38]. This trend could be because Ti has a higher thermal expansion coefficient than Ge, which affects the series resistance of the contact [39]. The thermal expansion coefficient of Ti for a 150 nm thick film is approximately 20 $\times$ 10^{-6}/ °C, while that of Ge is 6 $\times$ 10^{-6}/ °C. Consequently, since the Ti contact pad shrinks much more than the Ge, it reduces the contact area and influences the total current in the I-V measurements. Although this phenomenon is not widely studied, it is essential for understanding devices that experience temperature-sweeping conditions.

3.2. *Ti/Ni nano-island/n-Ge contact structure*

As mentioned above, a triple contact structure with two different metal species at a single contact can boost current flow. In order to fabricate a metal nano-island embedded contact structure that is compatible with conventional CMOS fabrication, Ni and Ti were deposited using DC sputtering. Ti and Ni were chosen due to their large work-function differences and widespread use in CMOS fabrication.

To create nano-scaled particles, Ni was sputtered for a short period of time. The resulting metal nano-islands were found to cluster on the Ge's surface due to the Ge's and Ni's surface energies, which induced the Ni atoms' clustered shapes during the initial deposition steps. If deposition continued longer, the Ni nano-islands would connect and form a

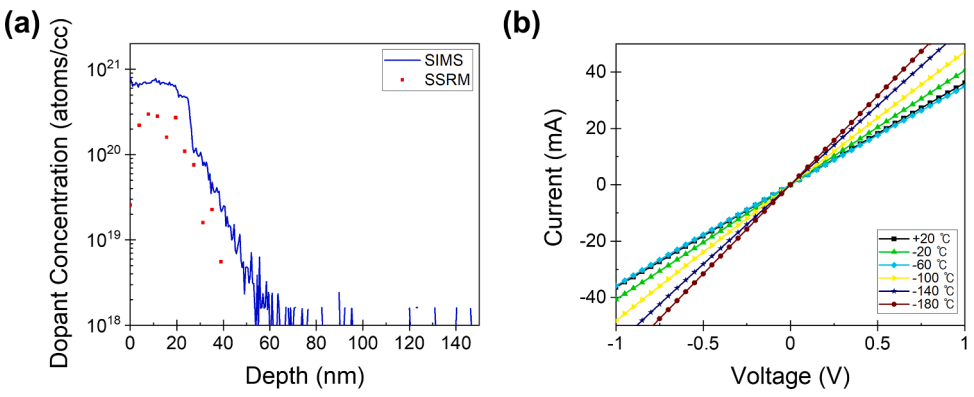

Fig. 5. (a) The comparison of ToF-SIMS and SSRM after 140 mJ/cm^2 of LAP. (b) I-V measurement of the activated Ge after LAP of 140 mJ/cm^2.

continuous Ni film on the Ge.

AFM analysis and a four-point probe method were used to determine the conditions necessary for Ni nano-island deposition. Not-activated Ge was used to ensure the substrate did not affect electrical results. The results obtained from three different deposition conditions are presented in Fig. 6 (a) and Fig. 6 (b). Fig. 6 (a) depicts the AFM images of the z-heights of bare Ge, after 7 s of sputtering, and 10 s of sputtering, respectively. The colors in all images were mapped using the same scale of −2 nm to 2 nm.

Fig. 6 (b) presents the AFM results of root mean square (RMS) roughness, peak-to-valley values, and Rs measurements. Before Ni deposition, the bare Ge surface showed a smooth profile without any noticeable features, exhibiting a peak-to-valley value of 1.602 nm, RMS roughness of 0.223 nm, and an error value of R_s that exceeded the maximum value of the instrument. The AFM analysis of the surface after 7 s of sputtering revealed rough spots, indicating non-uniform deposition of Ni. The peak-to-valley value and RMS roughness were measured to be 2.631 nm and 0.336 nm, respectively, indicating the non-uniformity of the deposited Ni film.

The R_s measurement showed an error value, suggesting that the deposited Ni was discontinuous. This non-uniformity is desirable since the Ti needs to be deposited as a contact to fill the gaps between the Ni nano-islands, forming a triple contact structure. After 10 s of sputtering, the surface became smooth without any roughness, with a peak-to-valley value of 1.504 nm and an RMS roughness of 0.213 nm, comparable to the values obtained for the bare Ge surface. At this point, the R_s was measured to be 2.18×10^6 Ω/□, indicating the continuity of the deposited Ni film, albeit with a very thin layer.

Following the deposition of the discontinuous Ni film, the Ti contact was deposited via DC sputtering while maintaining the vacuum. To examine the shape of the deposited Ni film, atomic distribution was obtained using Scanning Transmission Electron Microscopy (STEM). Fig. 7 (a) displays a STEM image, indicating that Ni atoms are arranged as nano-islands. These Ni nano-islands are circular and have a gap between them. As expected, the subsequent deposition of Ti filled the gaps between the Ni nano-islands. Energy-Dispersive X-ray Spectroscopy (EDS) was performed to measure the atoms' position. Fig. 7 (b) shows the result of the laterally scanned distribution, in a direction indicated by the arrow. As shown in the figure, the atomic counts of Ni increased when the Ti counts were low and decreased when the Ti counts were high. This observation indicates that the Ni nano-islands are embedded in the Ti contact, resulting in a triple contact structure.

Fig. 7 (c) shows the vertically scanned distribution results, which reveal that the island's height and diameter were around 3 nm without any significant increase in carbon (C) counts. The mapped results are shown in Fig. S4 (a). Supportive measurements by ToF-SIMS are shown in Fig. S4 (b), with embedded Ni peaks between Ti and Ge atoms. These observations confirm the triple contact structure was successfully fabricated.

3.3. Low specific contact resistivity with highly activated dopants and Ti/Ni nano-island contact

In order to evaluate the electrical properties of the triple contact structures, n^+-p diodes were fabricated. Three different contact metal sets, namely Ni, Ni nano-islands, and Ti (referred to as Ti/Ni nano-island in this study), and Ti, were deposited on the sample after LAP performed at a value of 140 mJ/cm^2. The top contact was patterned as 100 μm × 100 μm, and a 200 nm thick Al film was deposited at the bottom of the wafer.

The I-V characteristics of the n^+-p junction for the three different contact metal formations at room temperature are shown in Fig. 8 (a). Among the three conditions, the Ni nano-island contact showed the best result, exhibiting a high forward current density of 406 A/cm^2 at 1 V, higher than the other contact conditions.

Several factors contribute to the superior performance of the Ni nano-island contact. Firstly, as anticipated, the formation of Ni nano-islands resulted in an increased electric field between the metal and semiconductor layers. The work-function difference between Ti and Ni generated a supportive electric field that effectively lowered the Schottky barrier height [40–44]. In addition, Ni has a lower resistivity than Ti, resulting in lower series resistance and increasing the total current. Moreover, the Ni-only and Ti-only contacts also exhibited a high forward bias current, indicating successful activation of P with a high dopant concentration.

The calculated ideality factor showed three different regions following a typical trend of a diode [45]. The first region from 0 V to 0.25 V showed a lower value of slopes resulting in a high ideality factor of about 2. The reason is that the low bias voltage separated the electron and hole pairs, resulting in reduced forward current flow. The ideality factor from 0.25 V to 0.75 V showed the lowest indicating that the injection of carriers dominated the diode current. Lastly, from 0.75 V to higher junction voltages, the ideality factor starts to increase due to the parasitic components of the series resistance. Therefore, the ideality factor of the n^+-p junction diode with the Ni nano-island contact was calculated as 1.2 at the second region. This is due to the small bandgap of Ge, which implies that diffusion current was the dominant component of the flow. However, the on/off ratio of the diode was around two orders, primarily due to the high leakage current resulting in the narrow voltage margin for a well-behaved diode. The shallow junction with a high P concentration led to defects at the end-of-range, resulting in high leakage current [46].

As noted in a previous study, there is a trade-off between the fast diffusion nature of P in Ge. The high temperature annealing typically conducted for dopant activation and defect annihilation in shallow junctions with higher P concentration leaves defects, which cause high leakage current [47,48]. Therefore, the design of a Ge n^+-p junction diode must consider multiple factors, including dopant activation and annealing conditions, to optimize the trade-offs and minimize leakage

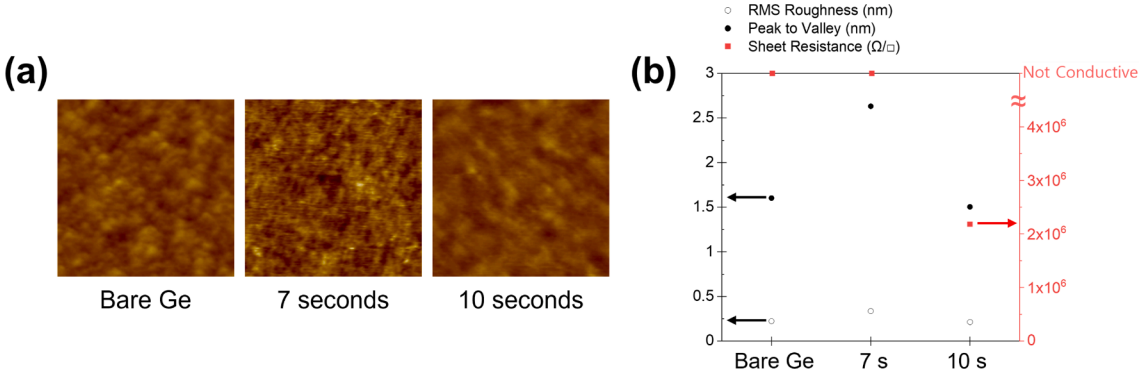

Fig. 6. (a) AFM results after the deposition of the Ni nano-island. Bare Ge before sputtering, 7 s, and 10 s after deposition samples were measured. (b) Measured RMS roughness, the Peak to Valley values of the AFM results, and the sheet resistance results are plotted for comparison.

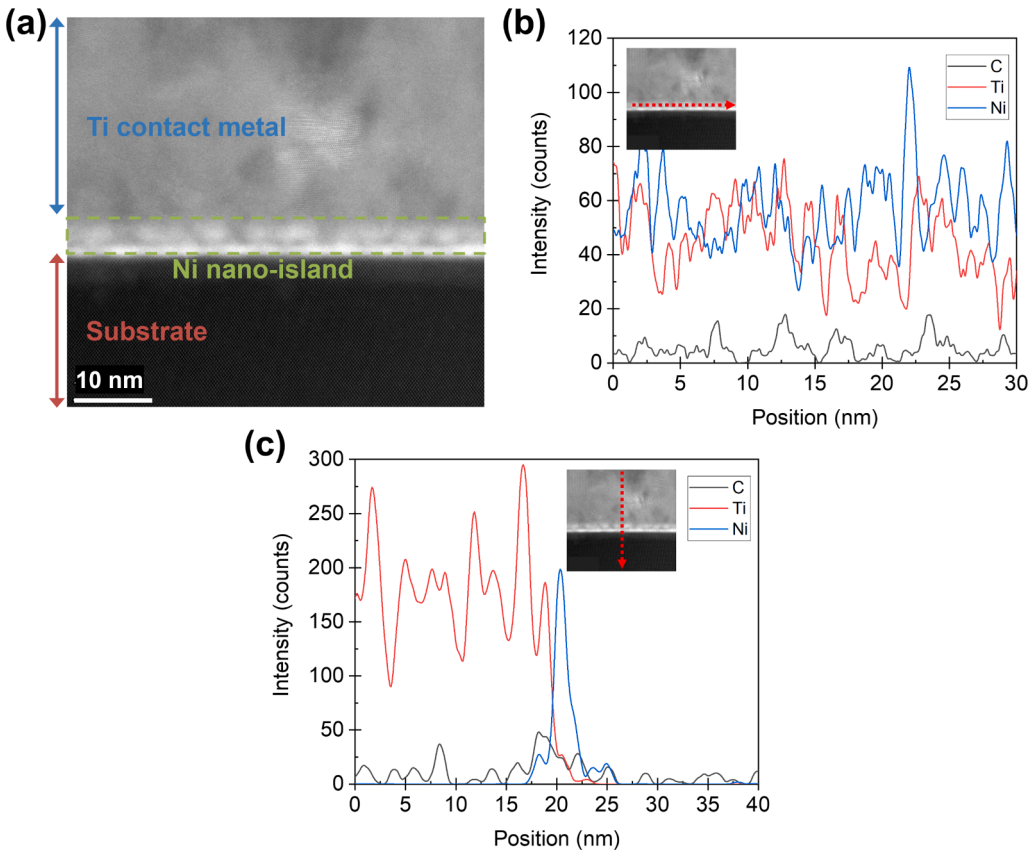

Fig. 7. (a) STEM image of the contact structure, with an embedded Ni nano-island after Ti contact formation. The Ni nano-islands appear as white atoms. (b) Lateral distribution of the atoms crossing a Ni nano-island. (c) Vertical distribution of atoms from Ti to the substrate.

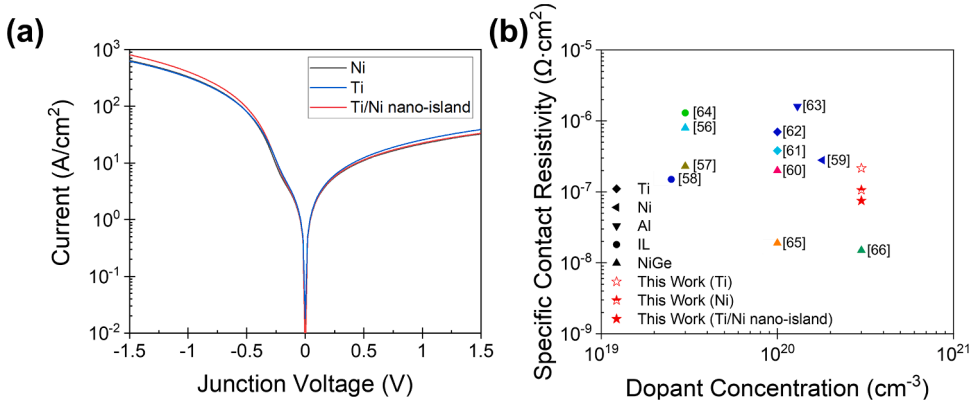

Fig. 8. (a) The I-V measurement results of the three different contact metal formations. (b) Specific contact resistivity as a function of dopant concentration for n-type Ge.

current [49–50]. In this point of view, there are related studies to reduce the leakage current. First, lowering the implantation temperature, called cold ion implantation, can reduce the leakage current with fewer traps and recombination centers [51]. Second, defectless doping processes avoiding collisions of ions to the substrate atoms minimize defects and are free of end-of-range damages [52,53]. Lastly, using higher purity and crystal quality of Ge wafer, which is under the limitation of manufacturing, can significantly improve the performance of devices.

Because the dopant concentration was as high as 3×10^{20} atoms/cm^3, the Schottky barrier height was extracted based on the I-V results at room temperature, assuming the thermionic emission model would not provide the exact value [54]. As the dopant concentration greatly affects the Schottky barrier, the exact value was underestimated and showed relatively low values [55]; 0.25 eV for the Ni and Ti contact and 0.23 eV for the Ti/Ni nano-island contact. However, even though the value was underestimated, the Ni nano-island contact formation reduced the Schottky barrier height by about 8 %.

Finally, the ρ_c of metal to activated Ge, treated by the LAP with 140 mJ/cm^2, was evaluated to determine the electrical property of the complete contact structure. It should be noted that the structure for Fig. 8 (b) consists of metal pads and n-Ge to extract the ρ_c between a metal contact pad and the underlying n-Ge. The structure of the MR-CTLM is shown in Fig. S5 (a). Fig. 8 (b) illustrates the benchmark of ρ_c as a function of dopant concentration [56–66]. The lowest ρ_c value was measured for the Ni nano-island contact, with a value of 7.5×10^{-8} Ω•cm^2. This result indicates that the highly activated P and the triple

contact of Ni nano-islands and Ti effectively increased the tunneling current. In Ni germanidation, the portion of the contact is very small, achieving even lower ρ_c values of around 1×10^{-8} Ω•cm^2 by lowering the Schottky barrier height [65,66]. However, Ni germanidation has several limitations, such as a rough surface due to the fast reaction of Ni and Ge, lack of thickness uniformity leading to significant variability in device characteristics, and doping profile modification. In contrast, the Ni nano-island embedded in the Ti contact demonstrated promising results compatible with conventional fabrication instruments.

The ρ_c values were also measured for a Ti only contact and Ni-only contact, which exhibited 2.15×10^{-7} Ω•cm^2 and 1.06×10^{-7} Ω•cm^2, respectively. The MR-CTLM measurement results are provided in Fig. S5 (b). Each point in Fig. S5 (b) is an averaged value of the measured sets. The ρ_c clearly showed trends of Schottky barrier resistance reduction, compared with other electrical analyses. Since the contact resistance is relatively smaller than the overall series resistance, including channel resistance, it can be easily ignored and underestimated in a saturated diode. However, the MR-CTLM structure extracts the ρ_c by removing other resistive factors, allowing an investigation of the specific contact. It also maximizes the contact area between metal and semiconductor compared to other methods, such as the transmission length method (TLM) and refined-TLM, ensuring highly precise ρ_c extraction. Finally, the observed reduction in ρ_c with Ni nano-islands further supports the improvement in the tunneling current of the Ti/Ni nano-island/n-Ge triple contact.

4. Conclusions

In conclusion, we have demonstrated the successful fabrication of n-type Ge diodes using a laser annealing process and a triple contact of Ti/Ni nano-island/Ge. Our electrical measurements and analyses confirmed the effectiveness of this approach, which resulted in significant improvements in both dopant activation and contact resistance. The LAP proved a powerful technique for activating dopants in Ge, achieving high dopant concentration and a uniform dopant profile. The optimal LAP energy density was 140 mJ/cm^2, which produced a dopant activation level of 3×10^{20} cm^{-3}.

The triple contact of Ti/Ni nano-island/Ge shows promise as a low-resistance contact for n-type Ge. The Ni nano-islands embedded in the Ti contact effectively increased the tunneling current, resulting in a ρ_c of 7.5×10^{-8} Ω•cm^2. This is a significant improvement compared to Ti-only and Ni-only contacts, which had ρ_c values of 2.15×10^{-7} Ω•cm^2 and 1.06×10^{-7} Ω•cm^2, respectively. In addition, the Ti/Ni nano-island/Ge contact is compatible with conventional fabrication instruments and can be easily integrated into existing processes for contacts of highly scaled devices.

We also analyzed the trade-offs involved in the design of n-type Ge diodes, particularly in the balance between dopant activation and annealing conditions. Our results showed that a shallow junction with a high P concentration leads to remaining defects that cause high leakage current, emphasizing the need to carefully consider the annealing conditions when designing junctions for n-Ge. This work provides insights into using LAP and Ti/Ni nano-island/Ge contacts to fabricate n-type Ge diodes. Our approach offers a promising path toward the development of high-performance Ge-based devices for CMOS applications.

CRediT authorship contribution statement

Seunghun Baik: Conceptualization, Methodology, Writing – original draft. **Heejae Jeong:** Data curation, Formal analysis. **Geuntae Park:** Visualization, Software. **Hongki Kang:** Investigation, Resources. **Jae Eun Jang:** Investigation, Resources. **Hyuk-Jun Kwon:** Supervision, Project administration, Funding acquisition, Writing – original draft.

Declaration of Competing Interest

The authors declare that they have no known competing financial interests or personal relationships that could have appeared to influence the work reported in this paper.

Data availability

Data will be made available on request.

Acknowledgements

This work was supported by the Samsung Electronics University R&D program and by the DGIST R&D Program of the Ministry of Science and ICT (23-CoE-BT-03). Also, this work was supported by the National Research Foundation of Korea (NRF) grants funded by the Korean government, MSIT (2022M3D1A2083618).

Appendix A. Supplementary material

Supplementary data to this article can be found online at https://doi.org/10.1016/j.apsusc.2023.157967.

References

[1] S. Salahuddin, K. Ni, S. Datta, The era of hyper-scaling in electronics, Nat. Electron. 1 (2018) 442–450, https://doi.org/10.1038/s41928-018-0117-x.
[2] R. Chau, S. Datta, M. Doczy, B. Doyle, J. Kavalieros, M. Metz, High-k/metal-gate stack and its MOSFET characteristics, IEEE Electron Device Lett. 25 (2004) 408–410, https://doi.org/10.1109/LED.2004.828570.
[3] M. Jurczak, N. Collaert, A. Veloso, T. Hoffmann, S. Biesemans, Review of FINFET technology, Int. SOI conference (2009) pp. 1-4. https://doi.org/10.1109/SOI.2009.5318794.
[4] K. Cheng, A. Khakifirooz, N. Loubet, S. Luning, T. Nagumo, M. Vinet, Q. Liu, A. Reznicek, T. Adam, S. Naczas, High performance extremely thin SOI (ETSOI) hybrid CMOS with Si channel NFET and strained SiGe channel PFET, Int. Electron Devices Meet. (2012) pp. 18.11. 11-18.11. 14. https://doi.org/10.1109/IEDM.2012.6479063.
[5] International Roadmap for Devices and Systems (IRDS™) 2021 Edition, https://irds.ieee.org/editions/2021, 2021.
[6] A. Toriumi, T. Nishimura, Germanium CMOS potential from material and process perspectives: Be more positive about germanium, Jpn. J. Appl. Phys. 57 (1) (2018) 010101.
[7] S.-h.C. Baek, Y.-J. Seo, J.G. Oh, M.G. Albert Park, J.H. Bong, S.J. Yoon, M. Seo, S.-y. Park, B.-G. Park, S.-H. Lee, Alleviation of fermi-level pinning effect at metal/germanium interface by the insertion of graphene layers, Appl. Phys. Lett., 105 (2014). https://doi.org/10.1063/1.4893668.
[8] V. Janardhanam, H.-J. Yun, I. Jyothi, S.-H. Yuk, S.-N. Lee, J. Won, C.-J. Choi, Fermi-level depinning in metal/Ge interface using oxygen plasma treatment, Appl. Surf. Sci. 463 (2019) 91–95, https://doi.org/10.1016/j.apsusc.2018.08.187.
[9] T. Nishimura, Understanding and Controlling Band Alignment at the Metal/Germanium Interface for Future Electric Devices, Electronics 11 (15) (2022) 2419.
[10] H. Jeong, Y. Kim, S. Baik, H. Kang, J.E. Jang, H.-J. Kwon, High and Uniform Phosphorus Doping in Germanium Through a Modified Plasma Assisted Delta Doping Process With H_2 Plasma Treatment, IEEE Electron Device Lett. 43 (2022) 1315–1318, https://doi.org/10.1109/LED.2022.3182730.
[11] S. Baik, H. Kwon, C. Paeng, H. Zhang, B. Kalkofen, J.E. Jang, Y. Kim, H.-J. Kwon, Boosting n-type doping levels of Ge with co-doping by integrating plasma-assisted atomic layer deposition and flash annealing process, IEEE Electron Device Lett. 40 (2019) 1507–1510, https://doi.org/10.1109/LED.2019.2931404.
[12] J. Kim, S.W. Bedell, D.K. Sadana, Improved germanium n^+/p junction diodes formed by coimplantation of antimony and phosphorus, Appl. Phys. Lett., 98 (2011) https://doi.org/10.1063/1.3558715.
[13] H.A. Tahini, A. Chroneos, R.W. Grimes, U. Schwingenschlögl, Co-doping with antimony to control phosphorous diffusion in germanium, J. Appl. Phys. 113 (7) (2013) 073704.
[14] H.A.W. El Mubarek, Reduction of phosphorus diffusion in germanium by fluorine implantation, J. Appl. Phys. 114 (22) (2013) 223512.
[15] S.-H. Huang, F.-L. Lu, C. Liu, Low contact resistivity (1.5×10^{-8} Ω-cm^2) of phosphorus-doped Ge by in-situ chemical vapor deposition doping and laser annealing, Int. Symp. on VLSI Tech., Systems and Application (VLSI-TSA), IEEE, (2016), pp. 1-2 https://doi.org/10.1109/VLSI-TSA.2016.7480526.
[16] S. Baik, D.-J. Kwon, H. Kang, J.E. Jang, J. Jang, Y. Kim, H.-J. Kwon, Conformal and ultra shallow junction formation achieved using a pulsed-laser annealing process integrated with a modified plasma assisted doping method, IEEE Access 8 (2020) 172166–172174, https://doi.org/10.1109/ACCESS.2020.3024636.

[17] R.R. Lieten, V.V. Afanas'ev, N.H. Thoan, S. Degroote, W. Walukiewicz, G. Borghs, Mechanisms of Schottky Barrier Control on n-Type Germanium Using Ge3N4 Interlayers, J. Electrochem. Soc. 158 (4) (2011) H358.

[18] M. Shayesteh, C.L.L.M. Daunt, D. O'Connell, V. Djara, M. White, B. Long, R. Duffy, NiGe Contacts and Junction Architectures for P and As Doped Germanium Devices, IEEE Trans. Electron Devices 58 (2011) 3801–3807, https://doi.org/10.1109/ted.2011.2164801.

[19] J. Vanhellemont, E. Simoen, On the diffusion and activation of n-type dopants in Ge, Mater. Sci. Semicond. Process 15 (2012) 642–655, https://doi.org/10.1016/j.mssp.2012.06.014.

[20] A. Chroneos, H. Bracht, Diffusion of n-type dopants in germanium, Appl. Phys. Rev. 1 (1) (2014) 011301.

[21] H.A. Tahini, A. Chroneos, R.W. Grimes, U. Schwingenschlögl, H. Bracht, Point defect engineering strategies to retard phosphorous diffusion in germanium, Phys. Chem. Chem. Phys. 15 (2013) 367–371, https://doi.org/10.1039/c2cp42973j.

[22] O. Gluschenkov, Z. Liu, H. Niimi, S. Mochizuki, J. Fronheiser, X. Miao, J. Li, J. Demarest, C. Zhang, C. Niu, FinFET performance with Si: P and Ge: Group-III-Metal metastable contact trench alloys, Int. Electron Devices Meet. (2016) pp. 17.12. 11-17.12. 14. https://doi.org/10.1109/IEDM.2016.7838437.

[23] Z. Liu, O. Gluschenkov, H. Niimi, B. Liu, J. Li, J. Demarest, S. Mochizuki, P. Adusumilli, M. Raymond, A. Carr, Dual beam laser annealing for contact resistance reduction and its impact on VLSI integrated circuit variability, Symposium on VLSI Technology (2017) pp. T212-T213. https://doi.org/10.23919/VLSIT.2017.7998175.

[24] B.C. Johnson, P. Gortmaker, J.C. McCallum, Intrinsic and dopant-enhanced solid-phase epitaxy in amorphous germanium, Phys. Rev. B 77 (2008), 214109, https://doi.org/10.1103/PhysRevB.77.214109.

[25] H. Bracht, Copper related diffusion phenomena in germanium and silicon, Mater. Sci. Semicond. Process 7 (2004) 113–124, https://doi.org/10.1016/j.mssp.2004.06.001.

[26] D. Brunco, K. Opsomer, B. De Jaeger, G. Winderickx, K. Verheyden, M. Meuris, Observation and suppression of nickel germanide overgrowth on germanium substrates with patterned SiO_2 structures, Electrochem. Solid-State Lett. 11 (2007) H39, https://doi.org/10.1149/1.2820441.

[27] H. Yu, M. Schaekers, T. Schram, W. Aderhold, A.J. Mayur, J. Mitard, L. Witters, K. Barla, N. Collaert, N. Horiguchi, A. Voon-Yew Thean, K. De Meyer, Low-resistance titanium contacts and thermally unstable nickel germanide contacts on p-type germanium, IEEE Electron Device Lett. 37 (4) (2016) 482–485.

[28] J. Sullivan, R. Tung, M. Pinto, W. Graham, Electron transport of inhomogeneous Schottky barriers: A numerical study, J. Appl. Phys 70 (1991) 7403–7424, https://doi.org/10.1063/1.349737.

[29] V. Narayanan, Z. Liu, Y.-M. Shen, M. Kim, E.C. Kan, Reduction of metal-semiconductor contact resistance by embedded nanocrystals, IEDM Tech. Dig. (2000) 87–90, https://doi.org/10.1109/IEDM.2000.904265.

[30] M.S. Gorji, K.Y. Cheong, Embedded nanoparticles in Schottky and Ohmic contacts: a review, Crit. Rev. Solid State Mater Sci. 40 (2015) 197–222, https://doi.org/10.1080/10408436.2014.940444.

[31] H.H. Gatzen, V. Saile, J. Leuthold, Micro and nano fabrication, Springer, Berlin, Heidelberg, 1 (2015) 2.

[32] D. Bäuerle, Laser processing and chemistry, Springer Science & Business Media, 2013.

[33] N. Chery, M. Zhang, R. Monflier, N. Mallet, G. Seine, V. Paillard, J.M. Poumirol, G. Larrieu, A.S. Royet, S. Kerdilès, P. Acosta-Alba, M. Perego, C. Bonafos, F. Cristiano, Study of recrystallization and activation processes in thin and highly doped Silicon-On-Insulator layers by nanosecond Laser Thermal Annealing, J. Appl. Phys. 131 (6) (2022) 065301.

[34] A. Cullis, H. Webber, N. Chew, Amorphization of germanium, gallium phosphide, and gallium arsenide by laser quenching from the melt, Appl. Phys. Lett., 42 (1983) 875-877 https://doi.org/10.1063/1.93798.

[35] M. Posselt, B. Schmidt, W. Anwand, R. Grötzschel, V. Heera, A. Mücklich, C. Wündisch, W. Skorupa, H. Hortenbach, S. Gennaro, M. Bersani, D. Giubertoni, A. Möller, H. Bracht, P implantation into preamorphized germanium and subsequent annealing: Solid phase epitaxial regrowth, P diffusion, and activation, J. Vac. Sci. Technol., B 26 (1) (2008) 430.

[36] X. Lu, D.D. Fanfair, K.P. Johnston, B.A. Korgel, High yield solution− liquid− solid synthesis of germanium nanowires, J. Am. Chem. Soc. 127 (2005) 15718–15719, https://doi.org/10.1021/ja055850z.

[37] E. Simoen, A. Brugere, A. Satta, A. Firrincieli, B. Van Daele, B. Brijs, O. Richard, J. Geypen, M. Meuris, W. Vandervorst, Impact of the chemical concentration on the solid-phase epitaxial regrowth of phosphorus implanted preamorphized germanium, J. Appl. Phys. 105 (2009) 093538 https://doi.org/10.1063/1.3125459.

[38] A. Kovalevskii, A. Dolbik, S. Voitekh, Effect of doping on the temperature coefficient of resistance of polysilicon films, Russ. Microelectron 36 (2007) 153–158, https://doi.org/10.1134/S1063739707030031.

[39] B. Sundqvist, V.K. Tolpygo, Saturation and pressure effects on the resistivity of titanium and two Ti-Al alloys, J. Phys. Chem. Solids 122 (2018) 41–50, https://doi.org/10.1016/j.jpcs.2018.05.046.

[40] V. Pavan Kishore, P. Paramahans, S. Sadana, U. Ganguly, S. Lodha, Nanocrystal-based Ohmic contacts on n and p-type germanium, Appl. Phys. Lett, 100 (2012) 142107 https://doi.org/10.1063/1.3700965.

[41] H. Zheng, B.K. Mahajan, S.C. Su, S. Mukherjee, K. Gangopadhyay, S. Gangopadhyay, Barrier modification of metal-contact on silicon by sub-2 nm platinum nanoparticles and thin dielectrics, Sci. Rep. 6 (2016) 1–14, https://doi.org/10.1038/srep25234.

[42] M.S. Gorji, K.Y. Cheong, Au nanoparticles embedded at the interface of Al/4H-SiC Schottky contacts for current density enhancement, Appl. Phys. A 118 (2015) 315–325, https://doi.org/10.1007/s00339-014-8733-4.

[43] O.I. Elmi, O. Cristini-Robbe, M.Y. Chen, B. Wei, R. Bernard, D. Yarekha, E. Okada, S. Ouendi, X. Portier, F. Gourbilleau, T. Xu, D. Stiévenard, Local Schottky contacts of embedded Ag nanoparticles in Al_2O_3/SiN_x: H stacks on Si: a design to enhance field effect passivation of Si junctions, Nanotechnol. 29 (28) (2018) 285403.

[44] Y. Abbas, A. Rezk, S. Anwer, I. Saadat, A. Nayfeh, M. Rezeq, M.d. Rezeq, Improved figures of merit of nano-Schottky diode by embedding and characterizing individual gold nanoparticles on n-Si substrates, Nanotechnol. 31 (12) (2020) 125708.

[45] W. Kim, W. Choi, A novel parameter extraction method for the one-diode solar cell model, Sol. Energy 84 (2010) 1008–1019, https://doi.org/10.1016/j.solener.2010.03.012.

[46] Y.-L. Chao, J.C. Woo, Germanium n^+/p Diodes: A Dilemma Between Shallow Junction Formation and Reverse Leakage Current Control, IEEE Trans. Electron Devices 57 (2010) 665–670, https://doi.org/10.1109/TED.2009.2039542.

[47] M. Shayesteh, D.O. Connell, F. Gity, P. Murphy-Armando, R. Yu, K. Huet, I. Toque-Tresonne, F. Cristiano, S. Boninelli, H.H. Henrichsen, P.F. Nielsen, D.H. Petersen, R. Duffy, Optimized Laser Thermal Annealing on Germanium for High Dopant Activation and Low Leakage Current, IEEE Trans. Electron Devices 61 (2014) 4047–4055, https://doi.org/10.1109/ted.2014.2364957.

[48] J. Kim, S.W. Bedell, D.K. Sadana, Multiple implantation and multiple annealing of phosphorus doped germanium to achieve n-type activation near the theoretical limit, Appl. Phys. Lett., 101 (2012) 112107 https://doi.org/10.1063/1.4751845.

[49] C. Wang, C. Li, S. Huang, W. Lu, G. Yan, M. Zhang, H. Wu, G. Lin, J. Wei, W. Huang, H. Lai, S. Chen, Phosphorus diffusion in germanium following implantation and excimer laser annealing, Appl. Surf. Sci. 300 (2014) 208–212, https://doi.org/10.1016/j.apsusc.2014.02.041.

[50] C. Wang, C. Li, G. Lin, W. Lu, J. Wei, W. Huang, H. Lai, S. Chen, Z. Di, M. Zhang, Germanium n^+/p Shallow Junction With Record Rectification Ratio Formed by Low-Temperature Preannealing and Excimer Laser Annealing, IEEE Trans. Electron Devices 61 (2014) 3060–3065, https://doi.org/10.1109/ted.2014.2332461.

[51] G. Margutti, P. Diego Martirani, M. De Biase, L. Latessa, M. Barozzi, E. Demenev, L. M. Rubin, C. Spaggiari, Silicon defects characterization for low temperature ion implantation and spike anneal processes, Int. Conference on Ion Implantation Tech., (2014), pp. 1-4. https://doi.org/10.1109/IIT.2014.6940014.

[52] S.-S. Chuang, T.-C. Cho, P.-J. Sung, K.-H. Kao, H.J.H. Chen, Y.-J. Lee, M.I. Current, T.-Y. Tseng, Ultra-Shallow Junction Formation by Monolayer Doping Process in Single Crystalline Si and Ge for Future CMOS Devices, ECS, J. Solid State Sci. and Technol. 6 (2017) P350–P355, https://doi.org/10.1149/2.0011707jss.

[53] K. Vanlalawpuia, B. Bhowmick, Investigation of a Ge-Source Vertical TFET With Delta-Doped Layer, IEEE Trans. Electron Devices 66 (2019) 4439–4445, https://doi.org/10.1109/ted.2019.2933313.

[54] S. Cheung, N. Cheung, Extraction of Schottky diode parameters from forward current-voltage characteristics, Appl. Phys. Lett. 49 (1986) 85–87, https://doi.org/10.1063/1.97359.

[55] J. Shannon, Control of Schottky barrier height using highly doped surface layers, Solid-State Electron. 19 (1976) 537–543, https://doi.org/10.1016/0038-1101(76)90019-8.

[56] A. Firrincieli, K. Martens, R. Rooyackers, B. Vincent, E. Rosseel, E. Simoen, J. Geypen, H. Bender, C. Claeys, J.A. Kittl, Study of ohmic contacts to n-type Ge: Snowplow and laser activation, Appl. Phys. Lett., 99 (2011). https://doi.org/10.1063/1.3666045.

[57] K. Gallacher, P. Velha, D.J. Paul, I. MacLaren, M. Myronov, D.R. Leadley, Ohmic contacts to n-type germanium with low specific contact resistivity, Appl. Phys. Lett. 100 (2) (2012) 022113.

[58] S. Gupta, P. Paramahans Manik, R. Kesh Mishra, A. Nainani, M.C. Abraham, S. Lodha, Contact resistivity reduction through interfacial layer doping in metal-interfacial layer-semiconductor contacts, J. Appl. Phys., 113 (2013). https://doi.org/10.1063/1.4811340.

[59] W. Hsu, F. Wen, X. Wang, Y. Wang, A. Dolocan, A. Roy, T. Kim, E. Tutuc, S. K. Banerjee, Laser Spike Annealing for Shallow Junctions in Ge CMOS, IEEE Trans. Electron Devices 64 (2017) 346–352, https://doi.org/10.1109/ted.2016.2635625.

[60] M.J.H. van Dal, B. Duriez, G. Vellianitis, G. Doornbos, M. Passlack, Y.-C. Yeo, C. H. Diaz, Germanium n-Channel Planar FET and FinFET: Gate-Stack and Contact Optimization, IEEE Trans. Electron Devices 62 (2015) 3567–3574, https://doi.org/10.1109/ted.2015.2477441.

[61] Z. Li, X. An, Q. Yun, M. Lin, M. Li, M. Li, X. Zhang, R. Huang, Low Specific Contact Resistivity to n-Ge and Well-Behaved Ge n^+/p Diode Achieved by Multiple Implantation and Multiple Annealing Technique, IEEE Electron Device Lett. 34 (2013) 1097–1099, https://doi.org/10.1109/LED.2013.2272641.

[62] G. Thareja, J. Liang, S. Chopra, B. Adams, N. Patil, S.-L. Cheng, A. Nainani, E. Tasyurek, Y. Kim, S. Moffatt, High performance germanium n-MOSFET with antimony dopant activation beyond 1×10^{20} cm^{-3}, Int. Electron Devices Meet., (2010) pp. 10.15. 11-10.15. 14. https://doi.org/10.1109/IEDM.2010.5703336.

[63] C. Wang, C. Li, S. Huang, W. Lu, G. Yan, G. Lin, J. Wei, W. Huang, H. Lai, S. Chen, Low specific contact resistivity to n-Ge and well-behaved Ge n+/p diode achieved by implantation and excimer laser annealing, Appl. Phys. Express 6 (10) (2013) 106501.

[64] J.-Y.-J. Lin, A.M. Roy, K.C. Saraswat, Reduction in Specific Contact Resistivity to n $^{+}$ Ge Using TiO_2 Interfacial Layer, IEEE Electron Device Lett. 33 (2012) 1541–1543, https://doi.org/10.1109/LED.2012.2214758.

[65] H. Miyoshi, T. Ueno, K. Akiyama, Y. Hirota, T. Kaitsuka, In-situ contact formation for ultra-low contact resistance NiGe using carrier activation enhancement (CAE) techniques for Ge CMOS, Dig. Tech. Pap. Symposium on VLSI Technology, (2014) pp. 1-2. https://doi.org/10.1109/VLSIT.2014.6894409.

[66] S.H. Huang, F.L. Lu, W.L. Huang, C.H. Huang, C.W. Liu, The $\sim 3\times10^{20}$ cm^{-3} Electron Concentration and Low Specific Contact Resistivity of Phosphorus-Doped Ge on Si by In-Situ Chemical Vapor Deposition Doping and Laser Annealing, IEEE Electron Device Lett. 36 (2015) 1114–1117, https://doi.org/10.1109/led.2015.2478916.